Histology and Histopathology
From Cell Biology to Tissue Engineering

ORIGINAL ARTICLE **Open Access**

The kidnapping of mitochondrial function associated with the SARS-CoV-2 infection

Elizabeth Soria-Castro[1]*, María Elena Soto[2]*, Verónica Guarner-Lans[3], Gustavo Rojas[4], Mario Perezpeña-Diazconti[1], Sergio A Críales-Vera[5], Linaloe Manzano Pech[1] and Israel Pérez-Torres[1]

[1]Cardiovascular Biomedicine, [2]Immunology, [3]Physiology, [4]Intensive Care Unit and [5]Computed Tomography Departments, Instituto Nacional de Cardiología "Ignacio Chávez", Tlalpan, México City, México

*These authors contributed equally to the work

Summary. Infection by the Severe Acute Respiratory Syndrome Coronavirus 2 (SARS-CoV-2) leads to multi-organ failure associated with a cytokine storm and septic shock. The virus evades the mitochondrial production of interferons through its N protein and, from that moment on, it hijacks the functions of these organelles. The aim of this study was to show how the virus kidnaps the mitochondrial machinery for its benefit and survival, leading to alterations of serum parameters and to nitrosative stress (NSS). In a prospective cohort of 15 postmortem patients who died from COVID-19, six markers of mitochondrial function (COX II, COX IV, MnSOD, nitrotyrosine, Bcl-2 and caspase-9) were analyzed by the immune colloidal gold technique in samples from the lung, heart, and liver. Biometric laboratory results from these patients showed alterations in hemoglobin, platelets, creatinine, urea nitrogen, glucose, C-reactive protein, albumin, D-dimer, ferritin, fibrinogen, Ca^{2+}, K^+, lactate and troponin. These changes were associated with alterations in the mitochondrial structure and function. The multi-organ dysfunction present in COVID-19 patients may be caused, in part, by damage to the mitochondria that results in an inflammatory state that contributes to NSS, which activates the sepsis cascade and results in increased mortality in COVID-19 patients.

Key words: SARS-CoV-2, Mitochondria, Electron transport chain, COVID-19, Nitrosative stress

Corresponding Author: Israel Pérez-Torres, Cardiovascular Biomedicine, Instituto Nacional de Cardiología "Ignacio Chávez", Juan Badiano 1, Sección XVI, Tlalpan, México City 14080, México. e-mail: pertorisr@yahoo.com.mx

Introduction

By the end of December 2019, an outbreak of a new infection caused by the Severe Acute Respiratory Syndrome Coronavirus 2 (SARS-CoV-2) was reported (Singhal, 2020). During this disease, as in other viral infections, an antiviral mitochondrial response is elicited to protect these organelles since they are essential to perform most of the catabolic processes required to produce ATP through the tricarboxylic acid cycle (TCAC) and the activation of the electron transport chain (ETC) (Pérez-Torres et al., 2020). Mitochondria are also a critical part of the antioxidant defenses since they contain in their matrix catalase, the isoforms of super oxide dismutase (SOD), thioredoxin 2, glutathione peroxidases (GPx) 1 and 4, glutathione (GSH) and α-keto acids. (Pérez-Torres et al., 2020). Finally, mitochondria also participate in the metabolism of pyrimidine, glutamine, urea, ammonia, and steroids (Mailloux, 2018).

Rupture of mitochondria results when the antiviral mitochondrial response is unable to counteract the viral infection and mitochondrial functions are disrupted. Many of the enzymes contained in these organelles are then released into the cytoplasm (Mailloux, 2018).

The antiviral mitochondrial response is initiated by the mitochondrial antiviral-signaling protein (MAVS), which is an adaptor molecule of the retinoic acid-inducible gene I (RIG-I). MAVS is localized in the mitochondrial outer membrane and it binds to the viral RNA to induce the production of interferons (IFNs) (Hee and Cresswell, 2017). The IFN system is the first line of defense against viral invasions (Koshiba et al., 2011). The degradation of MAVS inhibits the production of ATP by blocking the energy provision to the host and by decreasing the antiviral system, thus enhancing the viral infection (Paumard et al., 2002). However, several viruses may also evade the antiviral mitochondrial response by damaging the mitochondrial DNA (mtDNA)

(Yin et al., 2017).

COVID-19 is associated with a pro-inflammatory cytokine storm which blocks mitochondrial oxidative phosphorylation and is associated with a low production of ATP (Paumard et al., 2002). Although the cytokine storm is the host's response to eliminate the virus, it may damage the host, resulting in multi-organic failure (Soto et al., 2020; Chavarría et al., 2021).

Some of the structural and non-structural proteins that are encoded by the RNA genome of SARS-CoV-2 interact with mitochondrial components. Viral proteins enter the mitochondria as part of the strategy to kidnap the host's machinery and this constitutes a necessary step for the establishment of the infection (Jean-Beltran et al., 2017).

Although a few studies and computational models of SARS-CoV-2 have suggested that the viral RNA should be localized the in the mitochondria, since these organelles are one of the main targets of SARS-CoV-2 (Davies et al., 2020; Wu et al., 2020), there is still no physical evidence of the presence of the virus in the mitochondria. Therefore, the aim of this study was to show how SARS-CoV-2 may kidnap the mitochondrial machinery for its benefit generating important repercussions in the cells of the host.

Materials and methods

Ethics statement

This was an observational, comparative, and descriptive study that was performed in a prospective cohort of 15 postmortem patients affected by COVID-19 that attended the Instituto Nacional de Cardiología "Ignacio Chávez". The study was conducted in accordance with the principles of the declaration of Helsinki of 1964 and all procedures were in accordance with the ethical standards of the Institutional Research Committee. The protocol was approved by the Research and Ethics Committee of our institution (Institutional protocol number: 20-1157). In this study, an informed consent was obtained for medical care. For the postmortem study, an informed consent was requested and signed by the relatives. An informed consent for the publication of the data was obtained from participants, legal guardian(s), legally authorized representatives or next of kin (for dead patients).

Demographical data and Laboratory tests

Collected demographical data from the patient's medical history included, schooling, occupation, habits, illnesses prior to infection by SARS-CoV-2, test result for COVID-19, whether mechanical ventilation was used, and the type of treatment given. They were used for the analysis of the results. The laboratory tests included acute-phase reactants, hemoglobin, leukocytes, lymphocytes, platelets, glutamic, oxaloacetic transaminase (GOT), glutamic pyruvic transaminase (GPT), creatinine, urea nitrogen, glucose, C-reactive protein (CRP), albumin, D-dimer, ferritin, fibrinogen, Ca^{2+}, Cl^-, Na^+, K^+, pro-B-type natriuretic peptide (proBNP), lactate, troponin, and oxygen saturation.

Control subject

The histological results from the patients with COVID-19 were compared with those from a control subject, who was a 60-year-old female patient, negative for SARS-CoV-2. This patient had hepatocarcinoma, pulmonary micro-metastases and symptoms of pulmonary hypertension. There was no presence of degenerative disorders such as thyroid diseases, autoimmune diseases, or type 2 diabetes mellitus.

Obtainment of the post-mortem biopsies

The obtainment of the biopsy of the lungs, heart and liver was performed by ultrasound-guided minimally invasive autopsy, with precautionary measures for the protection of the health personnel. Standard protective equipment was used by the personnel to manage positive COVID-19 patients, including N95 mask, goggles, waterproof-gown and a double pair of gloves. Alcohol asepsis was performed on the area to be punctured to obtain the biopsy. The sample was obtained during the first 30 min after death of the patients and of the control subject. The heart, liver, and lung to be punctured were located by ultrasound using the SONOSCAPE X3 portable ultrasound machine with an X3 sector transducer. The average distance for the biopsy was measured, calculating the depth, which was found to be of 22 mm. A reusable tissue biopsy gun (BARD MAGNUM) was used. The heart was located using a four-chamber apical view with the patient in supine position. It was punctured under direct vision, orienting the disposable needle for biopsy (Magnum MN 1420, 16G x20cm) to the interventricular septum. Three punctures were made, seeking to obtain suitable material for the histological study and each sample was placed in a different bottle with 4% paraformaldehyde, 0.1% glutaraldehyde in 0.1 M PBS pH 7.4. The liver and heart biopsies were performed by placing the ultrasound in the right upper quadrant and mid axillary line, with the patient in supine position. Puncture was performed under direct vision with an average depth of 3 cm. Three samples were taken, trying to obtain adequate material. For the lung biopsy, punctures were performed at the apical and sub clavicular regions of the right, and left lung. The biopsy obtainment was guided by ultrasound at an average depth of 3 cm. A sample was taken from each puncture site.

Electron microscopy

For electron microscopy, small postmortem tissue

samples from the lung, heart, and liver of patients with COVID-19 and of the control subject were fixed with 2.5% glutaraldehyde for 1 hour and then stored in 0.1 M cacodylate buffer. Afterwards, they were post-fixed in 1% osmium tetroxide in 0.1 M cacodylate buffer (w/v). The samples were dehydrated in a graded series of ethanol and embedded in EPON 812 (Electron Microscopy Sciences). Ultrathin sections (60 nm in thickness) were cut using a ultracut microtome (RMC pt XL, Boeckeler Instrumentes Inc., Tucson, AZ. USA) and mounted on copper grids. Sections were contrasted with 3% uranyl acetate and 0.1% lead citrate and evaluated with a JEM-1011 (JEOL Ltd., Tokyo, Japan) at 80 kV, equipped with AMT 542.391 analysis software.

Immune colloidal gold technique

Small tissue samples of the lung, heart, and liver from the postmortem patients that had been infected with COVID-19 and of the control subject were processed according to the immune colloidal gold technique. Briefly, 1 mm tissue pieces were fixed for 2 hours in 4% paraformaldehyde, 0.1% glutaraldehyde in 0.1 M PBS pH 7.4. They were then washed three times with PBS/lysine solution (0.1 M sodium phosphate, sodium chloride 0.15 M and lysine 0.10 M, pH 7.4) at 4°C for 30 min. Afterwards, they were dehydrated in a graded series of ethanol at 4°C for 30 min. The infiltration was made progressively with a mixture that consisted of 1:3 and 1:2 ratio of ethanol/LR white for 3 h. They were then washed with LR only, for 3 hours, and incubated at 60°C. The samples were cut and mounted on carbon/formvar coated nickel grids. They were then incubated with antiserum for 1 hour, and with the primary antibodies diluted 1:20: Nitrotyrosine (HM.11), mouse monoclonal IgG_{2b}, sc-32731 (SantaCruz BioTechnology), COX II (D-5), mouse monoclonal IgM (kappa light chain), sc-514489 (SantaCruz BioTechnology) were used. Anti-COX IV, rabbit polyclonal antibody pAb, VB110-39115 (Wanleibio) and Anti-Caspase-9 rabbit polyclonal antibody, ab25758 (abcam) were also employed. Bcl-2 (N-19) rabbit polyclonal antibody sc-492 (SantaCruz BioTechnology), anti-MnSOD rabbit polyclonal antibody and IgG BIRBORB11394-100 (vwr) were used. Samples were incubated in a moist chamber at 4°C overnight. The samples were then washed 3 times for 10 min at 24°C, and incubated with a secondary antibody conjugated with colloidal gold diluted 1:20. The antibodies used were rabbit-anti-mouse gold 25 nm cat:25352 (Electron Microscopy Sciences), goat-anti-rabbit gold 15 nm cat:25112 (Electron Microscopy Sciences), and goat Anti-Mouse IgG 10 nm Gold, 10 OD, ab270536, (abcam) at 24°C for 3 hrs. Samples were washed with 0.1 M PBS and fixed with 2% glutaraldehyde. They were then stained with 3% uranyl acetate and 0.1 % lead citrate and evaluated with a JEM-1011 (JEOL Ltd., Tokyo, Japan) at 80 kV, equipped with AMT 542.391 analysis software.

Histological sections

For light microscopy, histological small sections of the tissue samples from the lung, left ventricle, and liver of the postmortem patients that died from COVID-19 and from the control subject were washed in 0.9% NaCl for 30 sec and fixed by immersion in phosphate buffer with 10% formalin (pH 7.4) for 24h. The sections were processed according to conventional histological procedures for the hematoxylin-eosin (H-E) stain. All photomicrographs were obtained with a Leica DM500 light microscope with a Plan 10x/0.22 NA and a Plan 40/0.065 NA objectives, with a digital camera for ICC50W/wi-fi microscope, (Leica).

X-ray plates

The conventional X-ray plates were taken from patients with COVID-19 in an anteroposterior position using a mobile portable-X Ray unit (Siemens, Erlangen

Table 1. Demographic Characteristics of the COVID-19 patients.

Age	47-74
body mass index	28.6±4.3
Weight by body mass index (%)	
Normal	4 (26.7)
Overweight	6 (40)
Morbid Obesity	5 (33.3)
Habits (%)	
Sedentarism	12 (80)
Alcoholism	5 (33.3)
Smoking	4 (26.7)
Marijuana use	1 (6.7)
Comorbid conditions prior to SARS-CoV-2 (%)	
Diabetes Mellitus	9 (60)
Systemic arterial hypertension	5 (33.3)
Ischemic heart disease	4 (26.7)
Dyslipidemia	3 (20)
Hypothyroidism	1 (6.7)
With valve prosthesis	1 (6.7)
Autoimmune disease (Systemic Lupus Erythematous)	1 (6.7)
Symptoms at the time of hospital admission (%)	
Dyspnea	13 (86.7)
Fever	12 (80)
Cough	7 (46.7)
Asthenia and adynamia	7 (46.7)
Myalgia	6 (40)
Arthralgia	5 (33.3)
Shaking chills	3 (20)
Odynophagia	3 (20)
Headache	3 (20)
Thoracic pain	2 (13.3)
Runny nose	2 (13.3)
Drowsiness	2 (13.3)
Diarrhea	1 (6.7)
dysuria and polyakiuria	1 (6.7)

Values indicate the number of patients having the condition and number in parenthesis represents the percentage of patients showing the condition. The informed consent for the publication of the data was obtained from participants /legal guardian(s)/legally authorized representative/next of kin (for dead patients).

Germany), together with a digital system (Flat panel).

Statistical analysis

Measures of central tendency and the normality test (Shapiro-Wilk) were used. Comparison of the independent variables were made by Mann-Whitney rank sum test, and the paired data were tested using the Wilcoxon sign-rank test. A p≤0.05 value was considered as statistically significant. The computer program SPSS version 19 (IBM Statistics, Armonk N.Y.) was used.

Results

Demographic characteristics

A total of 15 patients were examined, of which 12 were men (80%) and 3 were women (20%). Patients had an age range of 47-74 years. In them, infection by SARS-CoV-2 was diagnosed through CRP-tests, COVID-19-triage, Reporting and Data System (CO-RADS) and/or the score by computed tomography. The CRP-test was positive in 12 patients. In 3 patients there was not a confirmatory test; in two of them the test result was not collected after the death of the patients and in one, the test was negative. However, the pneumonia, the numerous days of the hospital stay and the lack of statistically significant differences in the laboratory test of these 3 patients when compared to patients with positive tests suggest they had COVID-19. Moreover, in the analysis by electron microscopy of the tissues, viral particles were present in tissues from these patients as in the patients with positive tests. The demographic characteristics of the patients are shown in Table 1. The average number of days of hospital stay was of 10 days with a minimum of two and a maximum of 35. Only one patient underwent a tracheostomy. During the evolution of the disease, 12 patients had acute renal failure, 2 had pulmonary thromboembolism, one patient had a myocardial infarction, and another had three-vessel ischemic disease with severe aortic and mitral regurgitation. In these last two cases, interventional treatment was warranted. 10 patients received mechanical ventilation, and in 7 of them, the measure was initiated at the time of admission, 1 a day later, 1 two days later and 1 three days after admission. 5 patients were only given supplemental oxygen treatment. The characteristics of previous diseases and organ failure and complications during the evolution of infection by SARS-CoV-2, are shown in Table 2.

Therapeutic antiviral management

The treatment applied during hospitalization was

Table 2. Characteristics of previous diseases and organ failure and complications during the evolution of infection by SARS-CoV-2.

		Characteristics and comorbidities prior to COVID-19														Patients who progressed to KF		
G	Age	OW/O	Alc	Smoke	DL	MD	SAH	H	IHD	HF	AD	BCr	FCr	BBun	FBun	KF	Test	Symptoms and other complications
M	50	+	-	-	-	-	-	-	-	-	-	1.1	4.05	34	75.5	+	+	Fever, chills, and dyspnea (PE)
M	49	+	-	-	-	-	-	-	-	-	-	0.83	1.6	13.9	26.4	-	+	Fever, odynophagia, arthralgia, and myalgia
M	67	+	+	+	-	+	+	-	-	-	-	0.9	5.7	29	126.2	+	+	Fever, chills, arthralgia, asthenia, and dyspnea
M	62	-	-	-	+	+	+	-	-	-	-	2.12	1.87	31	61.1	-	+	Fever, cough, headache, and dyspnea
M	55	-	+	-	-	-	-	-	+	-	-	1.4	3.2	20.7	70.3	+	+	Chest pain, asthenia and adynamia (AMI)
M	62	+	+	+	+	+	+	-	+	+	-	1.59	7.15	50.5	92.9	+	+	Fever, chills, chest pain, cough, asthenia, adynamia and dyspnea (AMI)
M	59	+	+	-	-	+	-	-	-	-	-	0.92	0.79	12	33.7	-	+	Fever, somnolence, asthenia, adynamia, myalgia and dyspnea
M	74	+	-	-	-	+	+	-	+	+	-	1.68	3.1	46	256	+	PR	Dyspnea and cardiogenic shock
M	56	+	-	+	-	-	-	-	-	-	-	1.04	4.05	16.3	67.2	+	-	Fever, odynophagia, rhinorrhea, asthenia, adynamia, myalgia and dyspnea
M	50	+	-	-	+	+	-	-	-	-	-	1.3	4.9	55.4	145.1	+	PR	Fever, odynophagia, cough, and dyspnea
M	66	+	-	+	-	+	-	-	-	-	-	1.08	2.98	28.2	58.2	+	+	Fever, somnolence, asthenia, adynamia, dyspnea and septic shock
M	57	+	+	-	-	-	-	-	-	-	-	0.9	1.06	16	19	-	+	Fever, cough, and dyspnea
F	58	-	-	-	-	+	-	-	-	-	-	0.4	4.13	12	96.9	+	+	Fever, cough, headache, asthenia, arthralgia, myalgia diarrhea, dyspnea
F	47	+	-	-	-	-	-	-	-	-	+	2.1	2.5	41.2	211	+	+	Fever, run nose, cough, arthralgia, myalgia, dysuria, and dyspnea
F	67	-	-	-	-	+	+	+	+	-	-	1.9	2.5	33	123	+	+	Cough and Dyspnea

G, Gender; M, male; F, Female; OW/O, overweight/Obesity; DL, dyslipidemia; MD, diabetes Mellitus; SAH, systolic arterial hypertension; H, hypothyroidism; IHD, ischemic heart disease; HF, heart failure; AD, autoimmune disease; BCr, baseline creatinine; FCr, final creatinine; BBun, baseline blood urea nitrogen; FBun, final blood urea nitrogen; KF, kidney failure; S, suspect; PR, pending result; PE, pulmonary embolism; AMI, acute myocardial infarction. ASAT, aspartate aminotransferase; GOT, glutamic oxaloacetic transaminase; AAT, alanine aminotransferase; GPT, glutamic pyruvic transaminase. The informed consent for the publication of the data was obtained from participants/legal guardian(s)/legally authorized representative/next of kin (for dead patients).

Lopinavir/ritonavir in 5 (33.3%), Lopinavir/ritonavir and angioplasty in 1 (6.7%), ivabradine in 2 (13.3%), tocilizumab in 1 (6.7%), hydrocortisone in 1 (6.7%), amikacin in 1 (6.7%) Levofloxacin in 1 (6.7%), vancomycin in 1 (6.7%) and angioplasty in 1 (6.7%). One patient was treated at home by a private doctor with acyclovir and the death happened on the same day of admission; therefore, he was only treated with resuscitation maneuvers and support medications. In 10 patients (66.6%) the diagnosis was viral pneumonia due to COVID-19 of which, 2 also had cardiogenic shock, 3 had septic shock, 2 ischemic heart diseases and 3 only pneumonia by COVID-19. Community-acquired pneumonia and septic shock was present in 2 (13.3%). 1 subject (13.3%) had respiratory distress syndrome and 1 patient was diagnosed with cardiogenic shock and acute myocardial infarction with suspected SARS-CoV-2 infection.

Laboratory tests

Table 3 shows the laboratory results on admission and at the time of death for the COVID-19 patients. Many of the patients were already showing changes in the different basal blood parameters when they were admitted, $p \leq 0.03$.

X-ray plates

The results of the representative X-ray plates are shown in Fig. 1A-D. These alterations were related with the histopathological changes in the lung Fig. 1E. There are changes that correspond to pneumonitis with increased thickness of the alveolar walls, capillary congestion, and hyperplasia of pneumocytes in the lung samples.

Histology

The histological results from the samples of the patients with COVID-19 were compared with those from control subject. The lungs in COVID-19 patients (Fig. 1), showed changes that correspond to pneumonitis. There was increased thickness of the alveolar walls, capillary congestion, and hyperplasia of pneumocytes that is indicated by arrowheads in the figures. There was moderate inflammatory infiltrate with polymorphonuclear leukocytes and alveolar macrophages which is indicated by arrows. Some cases also showed diffuse alveolar damage with activated fibroblasts, type II pneumocytes, hyaline membranes and a protein-rich exudate. In the small pulmonary arteries, there was also infiltrate of lymphocytes.

Representative photomicrographs of the heart from the control patient and from a COVID-19 patient are shown. The changes of cardiac hypertrophy are more marked in the COVID-19 patient as can be observed in Fig. 2. In the control subject, there were mild changes of cardiac hypertrophy with variability in the size and shape of the nuclei (arrow), and some nuclei with hyperchromatism. In comparison, the image in panel B corresponds to a representative photomicrograph of the heart tissue from a COVID-19 patient. A close-up of the vessel (arrowhead) showed hyperplasia of the wall with

Table 3. Laboratory levels on admission and at the moment of death of patients.

Reference value units	Laboratory results at admission Median (Min-Max)	Laboratory results at death Median (Min-Max)	p
Hemoglobin (11.7-16.3 g/dL)	14.5 (10-17.4)	10.8 (7.6-16.4)	0.001
Leucocytes (3.56-10.310^3/μL)	11;146 (4600-19900)	16173 (6400-25300)	0.03
Lymphocytes (0.99-3.2410^3/μL)	600 (100-1900)	600 (200-2100)	0.79
Platelets (150000-50000010^3/μL)	218000 (136000-314000)	180000 (113000-488000)	0.91
ASAT/GOT (13-39 U/L)	53.5 (6.5-131.2)	57.2 (13.5-549)	0.68
AAT/GPT (7-52 U/L)	36.7 (14-98)	41.5 (14-113)	0.97
Creatinine (0.6-1.2 mg/dL)	1.1 (0.40-2.1)	3.1 (0.79-7.15)	0.001
Blood urea nitrogen (7-25 mg/dL)	29 (12-55.4)	75.5 (19.25-256)	0.001
Glucose (70-105 mg/dL)	200 (98-648)	211 (30-471)	0.57
Creatinine phosphokinase (30-223 U/L)	244 (30-2701)	300 (58-6000)	0.15
Albumin (3.5-5 g/dL)	3.2 (2.2-4.1)	2.1 (1.6-3.3)	0.001
D-dimer (0-0.24 μg/mL)	315 (134-7150)	1666 (414-9567)	0.01
Ferritin (11-307 ng/mL)	876.5 (116-2291)	827 (201-15000)	0.59
Fibrinogen (1.9-5.13 μg/mL)	4.6 (3.2-7.10)	5.1 (4-7.8)	0.02
Ca^{2+} (8.6-10.3 mg/dL)	7.9 (6.7-9.4)	7.4 (6-9)	0.06
Cl^- (98-107 pg/mL)	98.5 (90-109)	102.5 (88-110)	0.03
Na^+ mmol/L (136-145)	132 (125-145)	136 (120-145)	0.22
K^+ (3.5-5.1 mmol/L)	4 (3.1-5.2)	5.3 (4.1-7.4)	0.003
pro-B-type natriuretic peptide (15-125 pg/mL)	899 (110-13420)	1857 (340-25000)	0.06
Lactate (0.5-1.6 mmol/L)	2 (0.80-6.40)	1.7 (1.1-8)	0.51
Troponin (8.4-18.3 pg/mL)	37 (8.2-690)	132 (8.6-27027)	0.001
C reactive protein high sensitivity (1-3 mg/L)	192 (1.4-563)	296 (55-480)	0.30

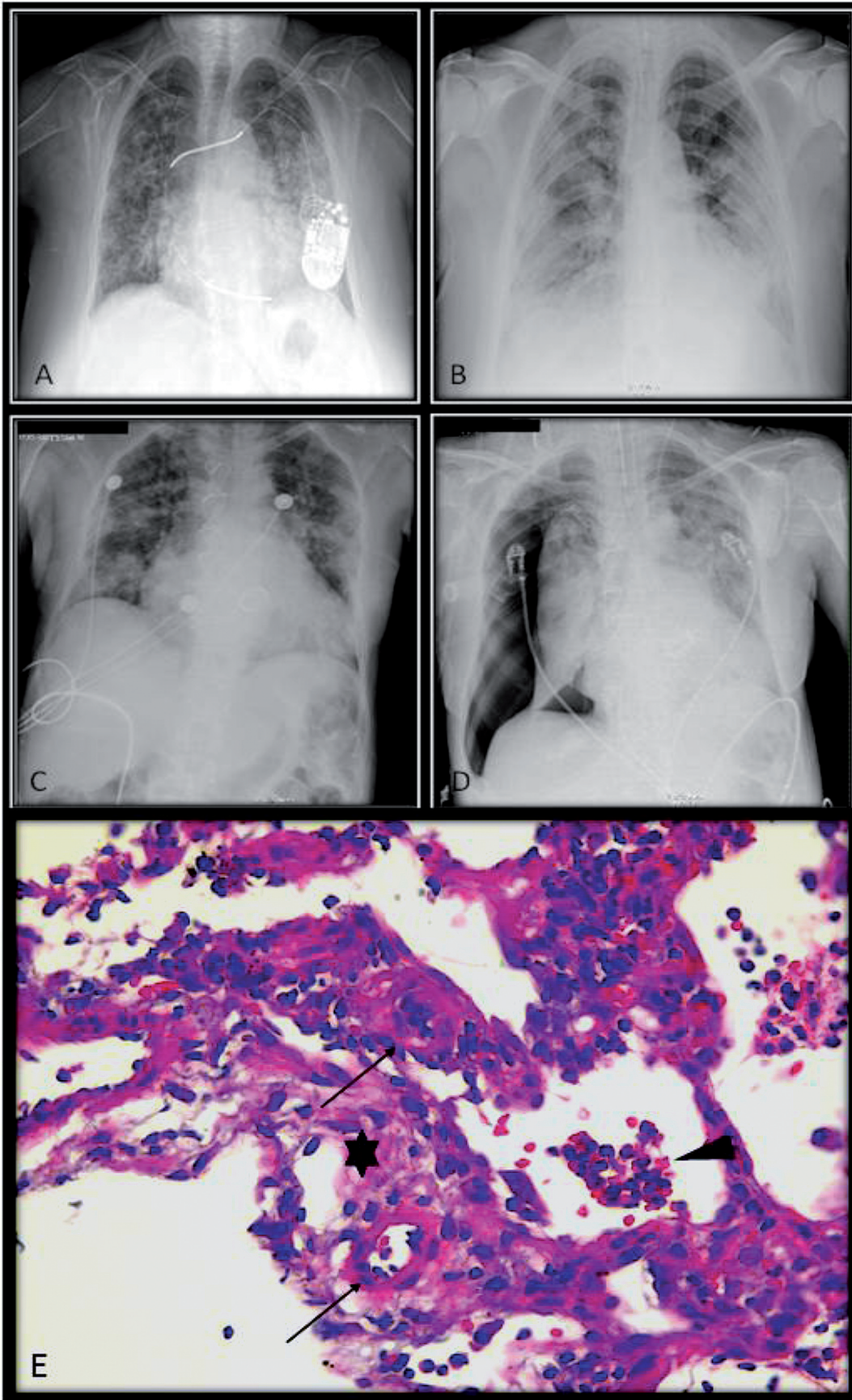The comparison it is between laboratories at admission vs. death.

Fig. 1. Representative X-ray plates and photomicrograph of lung tissue from a COVID-19 patient observed at 40x. Panel **A** corresponds to a 58-year-old female COVID-19 patient with bilateral hilar opacities predominantly on the left side and cardiomegaly. The presence of a defibrillator with the distal end projected in RV can be observed. Panel **B** corresponds to a 67-year-old female patient with diffuse opacities predominantly in the left perihilar region. An endotracheal tube in proper position can be observed, and panels **C** and **D** correspond to a 56-year-old male patient. The studies were separated by 7 days of evolution. In the initial image (**C**), perihilar opacities with predominance on the right side and on the posterior radiography are observed while in panel **D** a right pneumothorax and increased radiopacities on the left side can be seen. These alterations were related to the lung histopathological changes in panel **E**. Changes corresponding to pneumonitis are observed with hyperplasia of pneumocytes (indicated by arrowhead), with the presence of moderate inflammatory infiltrate of polymorphonuclear leukocytes and alveolar macrophages (indicated by arrows). There is also presence of a moderate inflammatory infiltrate of polymorphonuclear leukocytes and alveolar macrophages. Histological sections were made and stained by H-E and observed at 40x.

significant a decrease in lumen and inflammatory infiltrate of lymphocytes indicated by arrows. Cardiomyocytes showed degenerative vacuolization and inflammatory cells were not observed (40x). Patients with underlying cardiovascular diseases are at a higher risk of becoming infected with coronavirus, and the course of the disease is more severe in them than in patients without heart disease. Due to these clinical conditions, the changes of chronic diseases overlap with those of the SARS-CoV-2 virus, as shown in panel B. The patients with myocarditis showed an association with elevation of troponin and echocardiographic data.
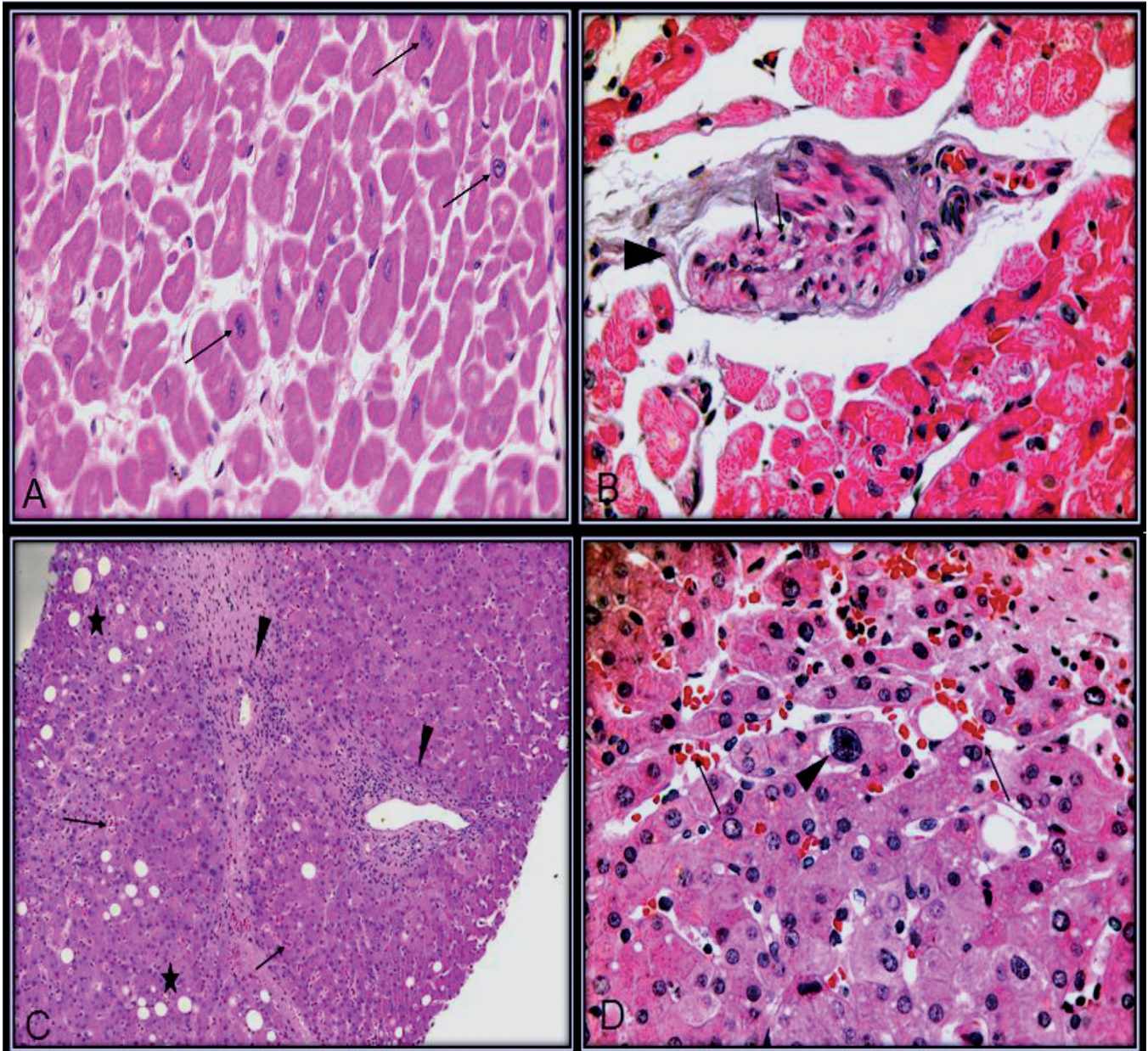
Fig. 2. Representative photomicrographs of heart and liver tissue from a COVID-19 patient and a control patient. Panel **A** corresponds to cardiac changes in a control patient. Mild changes of cardiac hypertrophy with variability in the size and shape of the nuclei (arrow), some with hyperchromatism. Panel **B**. Close-up of the vessel (arrowhead) shows hyperplasia of the wall with significant decrease in lumen and inflammatory infiltrate of lymphocytes indicated by arrows. Cardiomyocytes show degenerative vacuolization, and the inflammatory cells are not observed (40x). Panels **C** (10x) and **D** (40x) correspond to representative photomicrographs of liver tissue from a COVID-19 patient. The main changes observed in the liver are an increase in the inflammatory infiltrate by lymphocytes in the portal spaces which is indicated by an arrowhead, an increase in fibro connective tissue and steatosis indicated by a star, and congestion in the sinusoids indicated by arrows as shown in panel **C**). The arrowhead shows enlarged hepatocyte with finely granular cytoplasm. Histological sections were made with H-E stain.
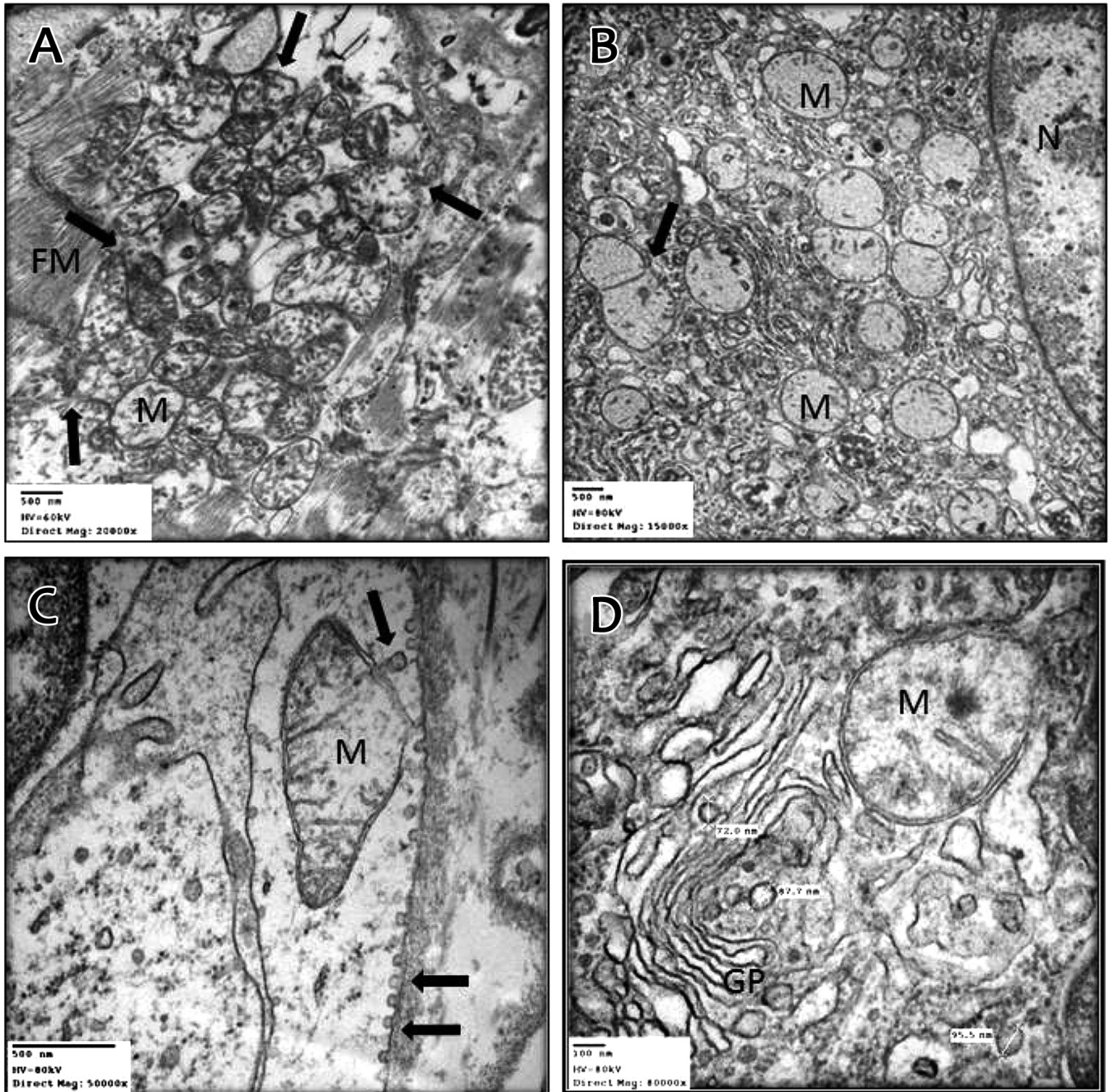
Fig. 3. Representative electron micrograph of different organs from COVID-19 patients at different magnifications. Panel **A**: heart (cardiomyocyte), **B**: liver (hepatocyte), **C** and **D** lung tissue (pulmonary hilum cell). Panel **A**: Interfibrillary mitochondria are shown with loss of continuity of the outer membrane. There are areas of mitochondrial fusion with loss of inner ridges and electro-dense areas in the fusion, but most are electro-lucid due to the loss of the matrix. Panel **B**: as in the heart, mitochondrial changes are maintained where mitochondrial fusion is shown again. Panel **C**: Lung macrophage where viral particles are observed in transition from the outer to the inner membrane; and a mitochondrion with loss of internal ridges and rupture of the external membrane is seen where there is a viral particle entering or leaving it. Panel **D**: Type II pneumocyte, where the Golgi apparatus and mitochondria with loss of internal ridges and the presence of viral particles are observed, which were measured. The viral particles were found ranging in size from 72 to 95.5 nm. FM, cardiac fibers; GP, Golgi apparatus; N, nucleus; M, mitochondria. Arrows, viral particles; Arrowhead, rupture of the external membrane mitochondrial. A, x 20,000; B, x 15,000; C, x 50,000; D, x 80,000.
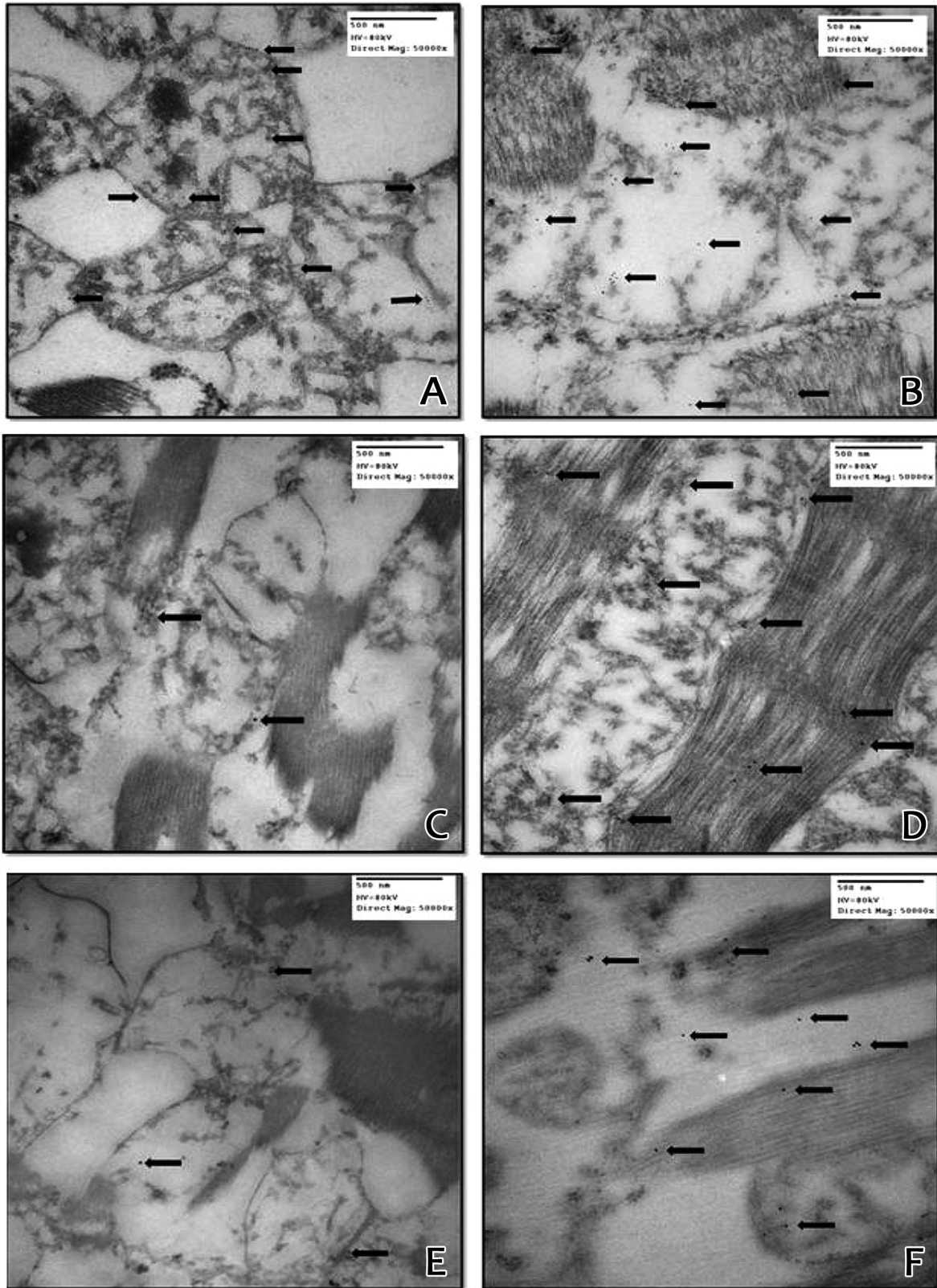
Fig. 4. Representative electron micrograph of heart tissue from: **A, C and E** = control subject, **B, D and F** = COVID-19 patient. In panels **A** and **B**, the arrows indicate the presence of the immune colloidal 10nm gold marker COX II in the sample from a COVID-19 patient. Membrane breaking is observed, and loss of the ridges of the inner membrane of the mitochondria. The subunit marker was present both on ridges and on the muscle fibers. This was not observed in the sample from the control. In panels **C** and **D**, the arrows indicate the presence of the subunit of the immune colloidal 15 nm gold marker for COX IV. There is a mitochondrion between cardiac muscle fibers in which the subunit marker was present both on ridges and the muscle fibers. In comparison, these changes were not observed in the control subject. In Panels **E** and **F**, the arrows indicate the presence of the immune colloidal 15 nm gold marker for MnSOD, which is an antioxidant enzyme. Mitochondria are present between cardiac muscle fibers. The electro-dense zone marker was present both on ridges and on the muscle fibers. In comparison, in the control subject, the electro-dense zones of the marker were only present inside the mitochondrial matrix. x 50,000.
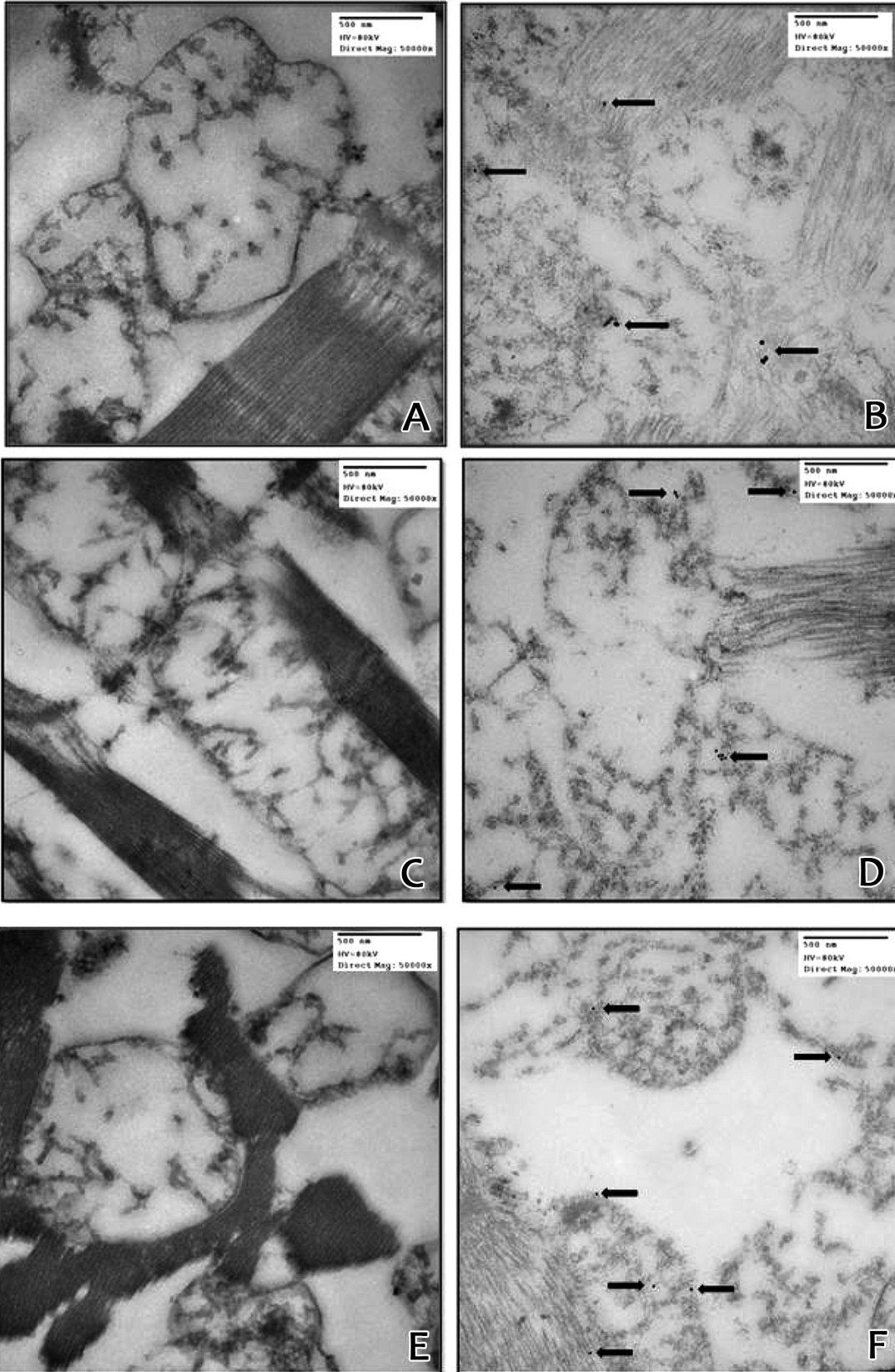
Fig. 5. Representative electron micrographs of heart tissue (cardiomyocytes) from: Panels **A, C and D** control subject, Panels **B, E and F** COVID-19 patient. In panels **A** and **B**, the arrows indicate the presence of the immune colloidal 25 nm gold marker for nitrotyrosine protein. There are mitochondria between cardiac muscle fibers and the electro-dense zone marker was present both on ridges and the muscle fibers. In comparison these changes were not observed in the control subject. In panels **C** and **D**, the arrows indicate the presence of the immune colloidal 15 nm gold marker for caspase 9. The electro-dense zone marker was present only in the mitochondria of the COVID-19 patients. The electro-dense zones were not present in the control subject. In panels **E** and **F**, the arrows indicate the presence of the immune colloidal 15 nm gold marker for Bcl-2 marker. Mitochondria are present between cardiac muscle fibers and the electro-dense zone marker was present only in the mitochondria from the COVID-19 patient. In the control subject, the electro-dense zones were not present. x 50,000.

In other patients with pre-existing cardiac disorders there are reports of ischemic cardiomyopathy with reduced LVEF.

Panels C (10x) and D (40x) correspond to representative photomicrographs of liver tissue from a COVID-19 patient. Preserved morphology was observed; however, there was an increase in the inflammatory infiltrate by lymphocytes in the portal spaces which is indicated by arrowheads. There was also an increase in fibro connective tissue, steatosis (indicated by star), and congestion in the sinusoids (indicated by arrows) in panel C). The arrowhead shows an enlarged hepatocyte with a finely granular cytoplasm. The cytopathic changes are apparent and there is an increase in the size of the nuclei which is at least four times bigger than the ones that surround it. Congestion in the sinusoids is indicated by arrows. In the liver, the columnar epithelial cells of the bile ducts did not show histological alterations (Panel D).

Electron microscopy

The electron microscopy of the cardiac tissue from COVID-19 patients showed alteration in the interfibrillary mitochondria with loss of the matrix and rupture of the ridges. In some cases, the rupture was in the outer membrane and, therefore, emptying of the mitochondrial matrix was observed (electron lucent
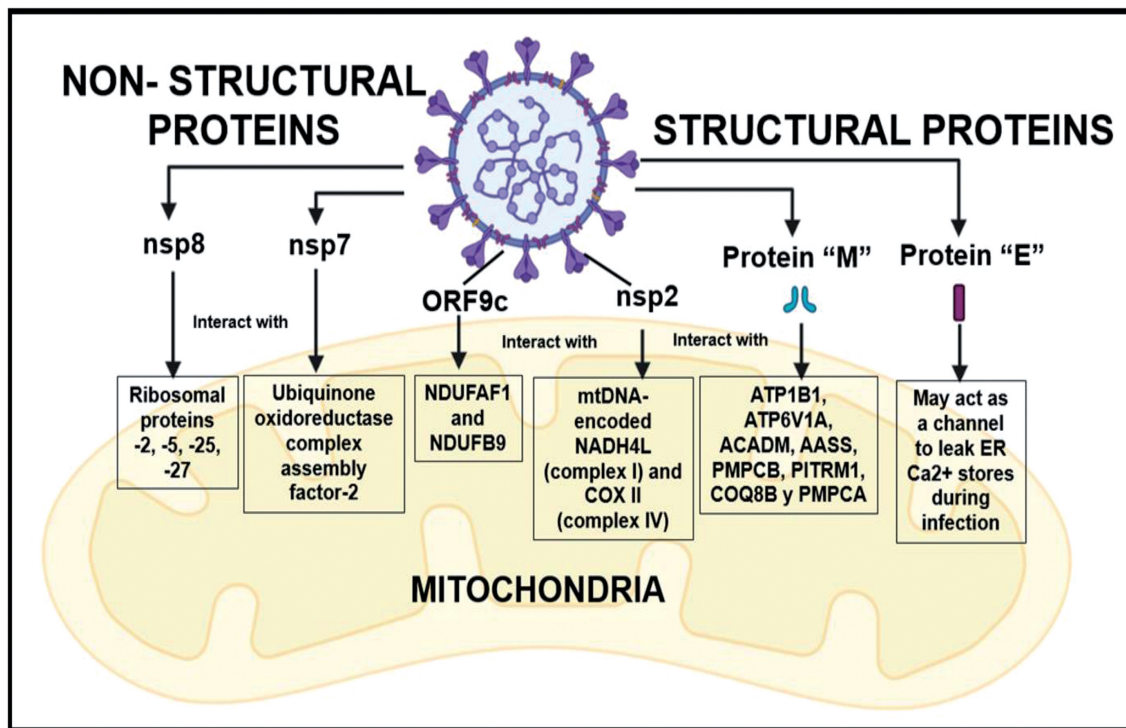

Fig. 6. Summary of the possible interactions of the different structural and non-structural proteins of the SARS-CoV-2 with the mitochondria. The RNA genome of this virus codes for structural and non-structural proteins. Four groups of proteins characterize the SARS-CoV-2. 1) viral envelope proteins (E) that include the spike structural glycoprotein (S) with prominent projections on the surface, the nucleocapsid (N) protein and the matrix protein (M), 2) proteases nsp1-nsp16, that participate as inhibitors of multiple steps of translation initiation (Lu et al., 2016), 3) a RNA-dependent RNA polymerase (RdRp) which is a non-structural protein and 4) a set of 4 or more 3' conterminal sub-genomic mRNAs replicase whose genes are composed of two overlapping open reading frames (Lu et al., 2016). The M protein determines the shape of the viral particle and binds to the nucleocapsid (Ibrahim et al., 2020), and can interact with ATP1B1, ATP6V1A, ACADM, AASS, PMPCB, PITRM1, COQ8B, and PMPCA, which are part of the critical metabolic pathways carried out in the mitochondria. Also, this protein may also interfere with the posttranscriptional machinery of the host by blocking the nuclear transport of spliced mRNAs and small nuclear RNAs and by slowing the nuclear transport of many other molecules. The E protein participates in viral particle release while the N protein interacts with the viral RNA to form the nucleocapsid and is responsible for distributing the viral ribonucleoprotein complex for replication; this protein may also promote the degradation of the MAVS, which acts as an adapter for transcription and production of IFNs being the most potent antiviral cytokine. The viral nsp are proteins that participate in synthesis or processing of viral RNA, or in virus-host interactions aiming to create an optimal environment for the replication of the coronavirus. The viral nsp8 may interact with mitochondrial ribosomal protein S-2, -5, -25, -27. The viral protein nsp7 may interact with the mitochondrial protein ubiquinone oxidoreductase complex assembly factor 2. The viral protein nsp2 can interact with the prohibiting protein PHB and nsp10 to interact with mtDNA-encoded NADH4L (complex I) and COX II (complex IV). The ORF9c can interact with the mitochondrial protein NADH dehydrogenase ubiquinone 1 α sub-complex assembly factor-1 (NDUFAF1) and NADH dehydrogenase ubiquinone 1 β sub-complex subunit-9 (NDUFB9). The NDUFB9 is an essential subunit of complex I and NDUFAF1 and -2 are critical players involved in the assembly of complex I. Abbreviations: NDUFAF1, NADH dehydrogenase ubiquinone 1 α sub-complex assembly factor-1; NDUFB9, NADH dehydrogenase ubiquinone 1 β sub-complex subunit-9.

mitochondria). Likewise, shortening and rupture of the cardiac fibers was observed (Fig. 3A). In the liver, vacuolization was observed in the cytoplasm of the hepatocytes and electron lucent mitochondria associated with the loss of the mitochondrial matrix are shown. In some areas, mitochondria were observed in a probable process of fusion (Fig. 3B). In the lung, infiltration was observed with the presence of viral particles associated with the inner membrane of alveolar macrophages. In some areas viral particles were observed in possible transition of fusion with the cell membrane. In addition, the mitochondria showed loss of the ridges and rupture of the outer membrane (Fig. 3C). In type II pneumocytes, the cisterns of the Golgi apparatus showed dilatation with the presence of viral particles. These particles were measured and had a diameter between 72 nm to 95 nm that corresponds to the reported range of the diameter of the SARS-CoV-2 (Fig. 3D). Furthermore, ultrastructural changes and gold marker for COX II, IV, MnSOD, nitrotyrosine, caspase 9 and Bcl-2

were observed in the COVID-19 patients and were compared with the control subject.

Immune colloidal gold technique

The results of the immune colloidal gold marker showed that COX II and IV were present in the cytosol, outside and inside the mitochondrial outer matrix of the heart tissue from COVID-19 patients (Fig. 4B,D). Furthermore, the mitochondria lacked the normal mitochondrial structural integrity. In comparison, the colloidal gold marker was present inside the mitochondrial matrix in the control subject (Fig. 4A and C respectively). Fig. 4F shows that the immune colloidal marker for MnSOD was present outside and inside the mitochondria in the samples from COVID-19 patients. In comparison, the mark was only found inside mitochondria in control subject Fig. 4E.

Fig. 5A,B show that the immune colloidal marker for nitrotyrosine was present outside and inside the
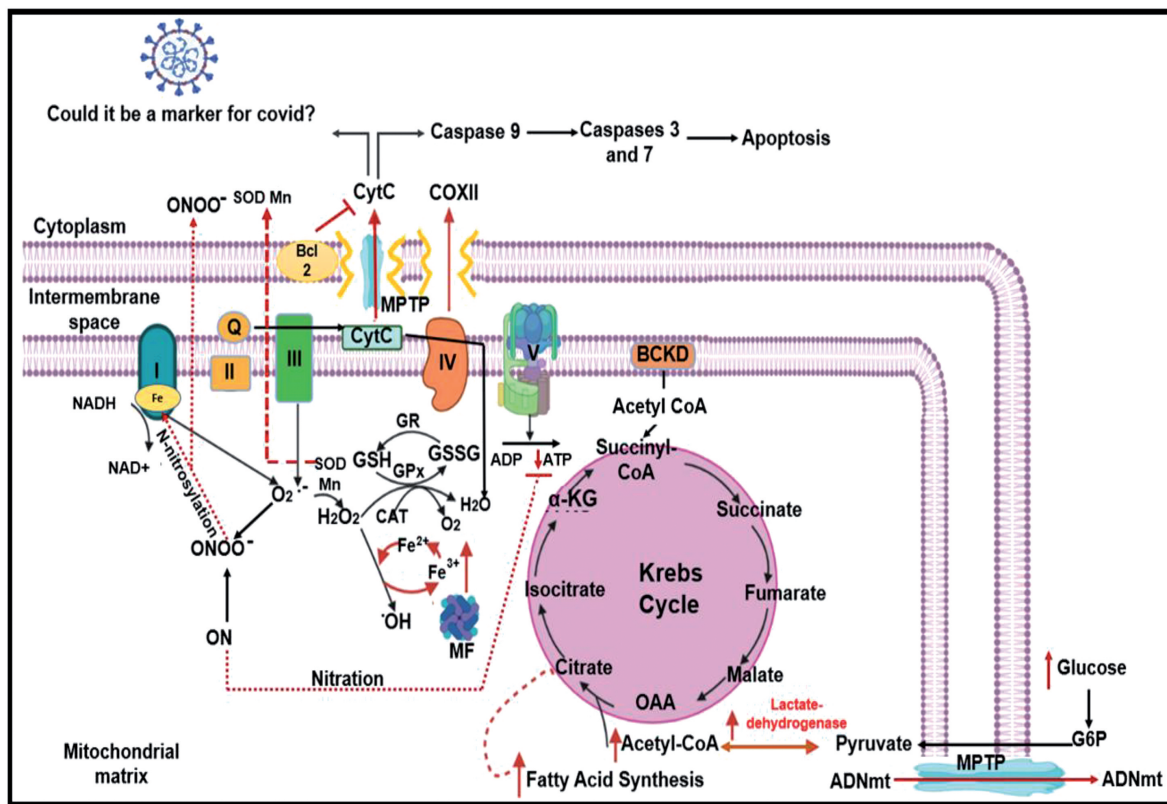

Fig. 7. Summary of mitochondrial alterations and possible damage caused by SARS-CoV-2. Viral envelope proteins E may act as channels to leak Ca^{2+} stores from the endoplasmic reticulum and other organelles during infection. The N viral protein mediates a ubiquitination process that degrades MAVS. The viral M protein interacts with critical mitochondrial metabolic pathways. Mitochondrial function is also regulated by the serine protease TMPRSS2 via the estrogen-related α-receptor, which transcriptionally regulates energy homeostasis. This protease is a key enzyme for the entry of SARS-CoV-2 into the host cells since it binds to the ECA2 receptor when it is linked to the virus through its S protein (Petersen et al., 2001). Abbreviations: Cyt c, cytochrome c; ONOO–, peroxynitrite; MPTP, mitochondrial permeability transition pore; SOD, superoxide dismutase; CAT, catalase; GPx, glutathione peroxidase; GR, glutathione reductase; GSH, glutathione; GSSG, oxidized glutathione; ON, oxide nitric; OH, hydroxyl radical; BCKD, branched chain keto acid dehydrogenase; α-KG, indicates α-ketoglutarate; OAA, oxaloacetate; G6P, glucose-6-phosphate; MF, mitochondrial ferritin.

mitochondria in the samples from COVID-19 patients (Fig. 5B). In comparison, the mark was only found inside mitochondria in the control subject (Fig. 5A). Figs. 5C,D show the immune colloidal marker for caspase 9 and Fig. 5E,F show the immune colloidal marker for Bcl-2 respectively. The mark was found inside the mitochondria in samples from COVID-19 patients. In comparison, electrodense zones were not present in the control subject.

Discussion

Mitochondrial defects have been implicated in numerous pathologies (including diabetes, cardiovascular diseases, gastrointestinal disorders, cancer, and aging) (Melser et al., 2015; Rumora et al., 2018) and mitochondria can also play an important role in viral infections. In viral diseases there is normally a mitochondrial evasive response. This is one of the first steps that the virus performs after it invades the host's cells, and it causes disruption of the mitochondrial function. Although SARS-CoV-2 hinders mitochondrial functioning, there is still no proof of its effects (Jean-Beltran et al., 2017). Therefore, the aim of this study was to show that the virus kidnaps the mitochondrial machinery for its benefit and survival. To prove this, we show that mitochondrial morphology is altered and that there is rupture of these organelles and presence of the viral particles in the mitochondrial matrix in samples from patients with COVID-19. These changes were not present in the control subject.

We show larger changes of cardiac hypertrophy and variability in the size and shape of the nuclei with some hyperchromatism and some alterations in the mitochondria in patients with SARS-CoV-2, in comparison with the control subject who only showed mild alterations. Many of the enzymes normally present inside the mitochondria are found in the cytoplasm of the cells of the different tissues from patients who died from COVID-19. Substrates and products from mitochondrial functions are altered in the serum of patients as a consequence of mitochondrial dysfunction and this may lead to multi-organic failure.

The results from our series of patients show that serum Ca^{2+} levels were low since their admission. This suggest that Ca^{2+} homeostasis could be altered in the mitochondria, ER and Golgi apparatus. The flux of Ca^{2+} released from ER and utilized by mitochondria can boost ATP production to meet a higher demand for energy due to constant viral replication (Zhou et al., 2009). However, later on, there is a decrease in the Ca^{2+} concentration both in the ER and Golgi apparatus which may contribute to inhibit protein trafficking pathways, decrease the antiviral response of the host, and prevent premature elimination by IFNs and the immune system (Davies et al., 2020). In addition, serological findings in critically ill COVID-19 patients with coagulopathy and thrombocytopenia show the presence of anticardiolipin IgA antibodies in serum. The presence of anticardiolipin

IgA antibodies suggests mitochondrial impairments associated with COVID-19. Cardiolipin is a mitochondrial phospholipid which participates in the maintenance of the structural integrity of the mitochondrial membrane where the proteins that make up the ETC are anchored (Zhang et al., 2020). The loss of structural integrity of the mitochondrial membrane may lead to release to the cytosol of iron-sulfur proteins (ISP) and Cytochrome C (Cyt c). The ISP constitute a family of electron transporters in the ETC. There are at least 6 iron-sulfur centers, in addition to cytochromes. These proteins have a heme group, consisting of a porphyrin ring and an iron atom which changes from state III to state II each time it accepts an electron. Cyt c or complex IV is an essential component of the ETC transferring electrons from complex III to complex IV. It plays a key role in the early events of mitochondria-mediated apoptosis (Sakaida et al., 2005). This complex consists of three subunits encoded by the mitochondrial genome (COX I, COX II and COX III) and ten subunits encoded by the nuclear genome (COX4, COX5A, COX5B, COX6A, COX6B, COX6C, COX7A, COX7B, COX7C and COX8). When Cyt c is released from the mitochondrial intermembranal space, it induces the activation of caspases (Malgorzata et al., 2020).

The results by immune colloidal gold marker show that COX II and IV were found in the cytosol and outside the mitochondrial outer matrix, and there was also a lack of mitochondrial structural integrity. In this sense, Cyt c liberation from the mitochondria into the cytoplasm is associated with the apoptosis protease-activating factor 1. It allows the recruitment of the initiator caspase-9 to form the apoptosome (Aubert et al., 2007). This phenomenon receives the term of intrinsic mitochondrial pathway (Huang et al., 2016). The formation of the apoptosome requires dATP/ATP and is critical for the activation of caspase 9. However, for this intrinsic pathway to be activated through the elevation of K^+ and Cl^- ion efflux, a low intracellular pH is needed (Segal and Beem, 2001) The results show an increase of the concentration of the K^+ and Cl^- ions in COVID-19 patients. Therefore, they suggest that the SARS-CoV-2 utilizes the intrinsic mitochondrial pathway for survival and replication.

Furthermore, the liberation of the ISP and heme group of the cytochromes can contribute to an iron deregulation manifested as hyperferritinemia in COVID-19 patients. Therefore, ferroptosis is present in patients leading to reductions in GPx4 and GSH. This results in an increase in lipoperoxidation and an elevation in the levels of hepdicin and ferritins (Arosio and Levi, 2002). The iron overload induces an increase in the intracellular labile iron pool accompanied with an excessive activation of heme oxygenase 1. In this sense, iron is sequestered by hepcidin in the enterocytes and macrophages leading to a decreased iron efflux from the cells. Ferroptosis is an important mechanism for pathogen proliferation and has also been described in HVB, HVC, HIV-1, cytomegalovirus, and SARS-CoV-2

(Jacobs et al., 2020). Therefore, there is a direct manipulation of iron homeostasis by the viruses causing an important imbalance. Recent clinical studies showed that iron metabolism is dysregulated in COVID-19 patients. Therefore, the ferroptosis in COVID-19 patients is likely caused by cell death and tissue damage, thereby releasing intracellular ferritin (Yang and Lai, 2020). Iron deregulation can also induce the production of reactive oxygen species (ROS) by the Fenton-Haber Weiss reaction and promote oxidative stress (OS) (Pérez-Torres et al., 2020; Chavarría et al., 2021). Both the iron overload and OS may be involved in platelet receptor activation that results in platelet dysfunction and a high rate of thrombosis (García-Yébenes et al., 2018). Appropriate mitochondrial functioning relies, in part, on iron uptake that is primarily utilized for storage in mitochondrial ferritin, in the iron-sulfur cluster for biogenesis and in the synthesis of heme groups (Paul et al., 2017). Hence, disruption of cellular iron levels or mitochondrial iron metabolism can result in cellular stress or death (Battaglia et al., 2020). Iron is transported by transferrin, the main protein that fixes the circulating iron. This ion cannot circulate in a free form because it causes OS. Iron is introduced to the cell by the receptors for transferrin and an intracellular iron excess causes mitochondrial abnormalities. Mitochondria are also focal hubs in iron metabolism and homeostasis. Mitochondrial iron participates in iron-sulfur cluster biogenesis and in heme synthesis. However, there is also a free and redox active iron pool which participates in the accumulation of mitochondrial ROS. Mitochondrial ROS react with PUFAs leading to lipid peroxidation, mtDNA damage, and subsequent defects in mtDNA-encoded subunits of the ETC complexes (Battaglia et al., 2020).

The hyperferritinemia observed in the COVID-19 patients may cause OS that leads to massive release of inflammatory mediators and ROS (Edeas et al., 2020). Also, the hyperferritenimia is a predictor of increased mortality of the disease (Delgado-Roche and Mesta, 2020), and can lead to a change in mitochondrial respiration from an aerobic to an anaerobic state. In this condition, pyruvate reduction into lactate is favored. This leads to an increase in lactate dehydrogenase, which is a highly up- regulated marker in COVID-19 (Young et al., 2020).

The results in this series of COVID-19 patients show that lactate is increased since their admission and remains high. This might reflect the degree of the anaerobic state in the mitochondria. Consequently, anaerobic mitochondria can result in a diminished cellular respiratory function. Dysfunctional mitochondria would result in iron accumulation due to their incapacity to metabolize it. This might cause a deficient iron sequestration, leading to ROS (Lane et al., 2015). Furthermore, there is an increase in lactate production in HCV-infected cells, due to kidnapping of the mitochondrial function by the virus, which then provokes an increased dependency on glycolysis in

hepatocytes (Ramiere et al., 2014). Besides, the increase in lactate is favored by a limiting rate of the available oxygen in a hypoxic state. In addition, an environment rich in glucose favors an imbalance in the electron gradient coming from the ETC, which leads to an increase in ROS (Herst et al., 2017).

Mitochondrial involvement in the survival of the virus is relevant since viruses require energy active processes for their life cycle (Glingston et al., 2019). Some viruses modulate the normal cell metabolism to increase aerobic glycolysis and to release the use of glucose for their bio-synthetical processes. Increased glucose elevates the pool of fatty acids and nucleotides that are needed by the viruses for their replication (Kapadia et al., 2005).

Our results show that plasma glucose levels were increased in this series of patients with COVID-19 since their admission, and levels remained high until the fatal outcome. This suggests that SARS-CoV-2 may increase aerobic glycolysis which contributes to the increase in glucose levels in blood. In this sense, diabetic people with elevated glucose levels are at an increased risk of developing the severe form of the COVID-19 illness. Elevated glucose levels and glycolysis promote SARS-CoV-2 replication and cytokine production in monocytes through mitochondrial ROS/hypoxia inducible pathway dependent on hypoxia inducible factor 1a. This factor is the transcriptional activator of several genes related to cellular adaptation to the hypoxic state which results in OS, severe inflammation, and cell death (Codo et al., 2020). In a hypoxic state, cells generally regulate the gene expression for proteins involved in glycolysis and in iron metabolism (Zhang et al., 2019).

In a diabetic state where OS is present, there is also an overstimulation of the adrenal glands, with an increase of the cortisol levels (Pal, 2020). In this sense, the SARS-CoV-2 causes viral amino acid expression of molecules that resemble adrenal corticotropic hormone (ACTH). Since there is a resemblance with the antibodies produced against the virus, these antibodies do not only bind to viral amino acid but also to host ACTH. This binding limits the host's ACTH functionality to stimulate secretion of cortisol in response to OS (Pal and Banerjee, 2020). Studies in autopsies of patients with SARS in 2003 showed degeneration and necrosis of the adrenal cortical cells. This suggests that the SARS-CoV family directly alters the dynamics of cortisol and causes relative adrenocortical insufficiency. This dysregulation of the cortisol has also been observed in COVID-19 patients (Pal, 2020).

Several stages of the replication cycle of the coronavirus are strongly associated with ER and mitochondrial stress. Indeed, expression of several coronavirus proteins, including the heavily glycosylated S protein, induces ER stress (Chan et al., 2006). Furthermore, the cytokine storm can induce a Ca^{2+}-dependent increase in the mitochondrial ROS, creating a

positive feedback loop, which directly unbalances the activity of the ETC, stimulating the production of proinflammatory cytokines (Li et al., 2013). This may cause mitochondrial membrane permeabilization, altered mitochondrial dynamics, and might ultimately result in cell death by apoptosis (Mittal et al., 2014). Also, an increase in ROS can be subsequently accompanied by reduced mitochondrial manganese which may result in mitochondrial dysfunction, and mainly in a low activity or expression of MnSOD. This enzyme protects the mitochondria from ROS that are generated by the respiratory process (Jouihan et al., 2008). The results in this study show that the localization of the MnSOD was not within the mitochondria, but outside it. This suggests that this enzyme may not be playing an adequate function in the detoxification of the ROS, and this can lead to a process of oxidation of mitochondrial proteins.

Damage to proteins might be caused by the virus S-nitrosylation that is the result of an excess production of ONOO−. This molecule is a secondary metabolite of the oxidation of nitric oxide, and its presence is associated with overproduction by the inducible nitric oxide synthase in a state of chronic inflammation (Pérez-Torres et al., 2020; Soto et al., 2020). ONOO⁻ may inactivate different mitochondrial proteins, including ETC components and TCAC dehydrogenases and this decreases the ATP levels (Pérez-Torres et al., 2020). Our results show that the localization of the labeling of S-nitrosylation proteins occurs both inside and outside of the mitochondria. This suggests that in COVID-19 patients, there is presence of NSS, probably resulting from the chronic inflammation associated with the cytokine storm.

Mitochondria actively communicate with the cytosol and nuclear compartments. Proteins located in the mitochondrial membrane, including the mitochondrial permeability transition pore (MPTP) help in the signaling involved in this communication process (Kwong and Molkentin, 2015). The products from the action of the ETC, such as ATP and Cyt c, are transferred to the cytosol to exert their biological functions through the MPTP and many viral proteins may alter the MPTP (Williamson et al., 2012). Alterations of the MPTP leads to passive swelling, outer membrane rupture, osmotic water flux, and release of pro-apoptotic factors leading to cell death (Anand and Tikoo, 2013). For example, HCV can induce the MPTP opening, regulating the release of mitochondrial contents such as mtDNA and Cyt c (Rongvaux et al., 2014). Furthermore, in an OS condition or cell damage by infection, mtDNA leaks out into the cytoplasm and it triggers inflammation and anti-viral responses, which involve the AIM2 and/or endosomal/extracellular toll-like receptor 9 (Mills et al., 2017). However, the liberation of the mtDNA levels and Cyt c increase the severity and progress of the infection and correlate with the onset of multi-organ failure in patients affected by acute respiratory distress (Simmons et al., 2017). This

suggests that the SARS-CoV-2 can manipulate the release of mtDNA and Cyt c, which participate in the inflammatory process (Singh et al., 2020), permeabilization of the mitochondrial membrane, and activate the apoptosome leading to cell death (Guler et al., 2020). The apoptosome activates the caspase cascade which begins with the activation of caspase 9 followed by caspase 3 (Hartmann et al., 2001). Our results show that labeling of caspase 9 occurred in the mitochondria.

However, in the eagerness of the host cell to protect itself from this increase in the apoptotic process, the host tries to activate alternative protective metabolic pathways such as the expression of the protein Bcl-2 (Luna-López et al., 2008). The Bcl-2 protein is a 26 kDa protein that is anchored to the outer membranes of the nuclear cisterns, the ER, and the outer membrane of the mitochondria. It is anchored to the mitochondrial membrane and is linked to anti-apoptotic properties. Bcl-2 participates in the preservation of the integrity of the mitochondrial membrane, in the prevention of the Cyt c release and in the activation of the caspases cascade. In addition, the expression of this protein decreases the levels of ONOO⁻ during periods of OS and stimuli that generate apoptosis (Luna-López et al., 2008).

Our results show that the localization of the labeling of Bcl-2 occurred in the mitochondria. This suggests that Bcl-2 expression is a mechanism of host protection to decrease the apoptotic process and oxidizing background. In addition, the localization of the nitrotyrosine labeling that appeared in the outer and inner membrane of the mitochondria suggests that infection by SARS-CoV-2 may induce NSS associated with the increase in hyperferritinemia that results from the release of Cyt c and ISP. This also contributes to the expression of Bcl-2. In addition, the apoptotic process is a trigger for the elevation of the D-dimer in COVID-19 patients (Guler et al., 2020). The results show that the D-dimer, troponin, and fibrinogen were increased from admission and that their levels remained high until the fatal outcome. The fibrinogen and troponin increase can be due to the double protective function they play, regulating the antiviral function of the immune cells, and assisting the host protective formation of fibrin matrices or clots that serve as barriers that limit the spread of the virus (Thachil et al., 2020). However, this condition results in coagulation abnormalities that are associated with a substantial COVID-19 mortality rate (Levi et al., 2020).

On the other hand, the ultrastructural changes and gold marker for COX II, IV, MnSOD, nitrotyrosine, caspase 9 and Bcl-2 observed in the COVID-19 patients and the control subject do not correspond to postmortem alterations of the tissue, because the time to obtain the biopsies was short (30 min). Therefore, these alterations may be typical of the infection by SARS-CoV-2. Also, the ultrastructural changes in the control subject are typical of the pathology that the subject was experiencing and do not correspond to the changes

observed in COVID-19 patients. This suggests that the host cells trigger these processes in the mitochondria, to protect themselves from kidnapping by the SARS-CoV-2. In this sense, several studies show that Cyt c liberation in postmortem tissue is present after two hours, without there being changes in the Bcl-2 (Huang et al., 2016), and in the thalamus degeneration after a cerebral stroke the Cyt c is released, in this condition the levels of Cyt c are detected to 5 days after the lesion and the expression of the RNA for Bcl-2 is decreased since day 3 (Onoue et al., 2005).

However, mitochondrial morpho-dynamics can also regulate the respiratory rate, and constitute a target used by SARS-CoV-2 to corrupt the mitochondrial metabolism and evade the immune response (Khan et al., 2015). Alterations in mitochondria also increase NDUFS2 that regulates the potassium channels sensitive to oxygen and the voltage-gated Ca^{2+} channels initiating pulmonary vasoconstriction. This leads to the presence of stiff and fibrotic pulmonary arteries Hyaline membranes in the alveoli are a prominent feature of lungs from patients with COVID-19, and dyspnea is profound (Archer et al., 2020). It is evident in the X-ray plates and by histopathological changes in lung tissue in our series of patients.

The inadequate cellular oxygen supply results in alterations in the TCAC and uncoupling of the ETC, leading to a decrease in the proton gradient (Levy and Deutschman, 2007), which results in production of heat rather than the generation of ATP (Brealey et al., 2002). This could contribute to increase the temperature in COVID-19 patients.

Furthermore, patients showed elevated levels of urea nitrogen since their admission and the levels further increased at the time of death. This may be due to poor blood flow distribution and low peripheral vascular resistance, especially at the microcirculatory level, which in turn results from inflammation and endotoxemia (Ince, 2005).

The results show that albumin was decreased. The mean value found at admission and compared with that of the final state of the patient was statistically significant. This confirms that in patients with sepsis, there is nutritional deterioration which progresses rapidly. The elevated level of CRP found at admission remained equally elevated until the time of death and the same was found with ferritin. CRP is produced in the liver and rises when there is a severe inflammatory state. It is also worth noting that in the case of a persistent inflammatory state, an increase in fibrinogen is found. Fibrinogen, like CRP and ferritin, is an acute phase reactant of inflammation and it was increased during the evolution of the patients in this series. Although the inflammatory state is relevant in these patients, the most relevant data was the deterioration of the renal function. This was demonstrated by the increase in serum creatinine and urea nitrogen, which goes hand in hand with the elevation of inflammatory markers from the liver and impaired mitochondrial

function.

Conclusions

The multi-organic dysfunction present in COVID-19 patients may be, in part, due to damage to the mitochondria that results in an inflammatory state. Mitochondrial damage renders these organelles dysfunctional, and they are then unable to meet the hyper metabolic demands caused by SARS-CoV-2. The alteration of the mitochondrial proteins can result in damage that inactivates innate immunity. Also, these alterations contribute to the elevation of ROS and NSS that activate the hyper inflammatory state and the deregulation of the OS thus contributing to the increased mortality. Figures 6 and 7 describe the kidnapping of the mitochondrial function and damage associated with SARS-CoV-2 infection.

Perspectives

The results observed in this study suggest that many of the alterations in the mitochondria can be decreased by a combined therapeutic strategy (Soto et al., 2020). The first phase of this strategy would be to lower the viral load that is the source and origin of the chronic inflammatory condition leading to severe sepsis, multiple organ failure and mitochondrial damage. The second phase should be aimed at decreasing alterations in the mitochondria which may be lowered by the use of antioxidants that have the capacity of restoring and protecting the mitochondrial function (Aisa-Alvarez et al., 2020; Soto et al., 2020; Chavarría et al., 2021). With respect to ferroptosis, this could also be a potential target in the treatment of COVID-19 since the use of iron chelators such as desferrioxamine and deferiprone might inhibit DNA synthesis in proliferating cells (Simonart et al., 2002). In addition, the use of direct-acting antivirals, in particular, the nucleoside/nucleotide analogues such as the remdesivir can efficiently inhibit viral replication by inhibiting the viral polymerase activity. However, these drugs may exert off-target effects by inhibiting mitochondrial DNA polymerase, resulting in a reduction of the number of copies of mtDNA (Qu et al., 2019). Finally, treatment with metformin as an adjuvant therapy might reduce the severity and mortality in COVID-19 (Luo et al., 2020).

Study limitations

The main limitation of this study was the obtainment of postmortem samples from patients with COVID-19. The technique for obtaining biopsies through an ultrasound-guided technique is minimally invasive and specific; however, the obtention of biopsies from brain or bone is not possible. It should be mentioned that it is not possible to perform a complete autopsy in patients that died from COVID-19 due to the risk that this implies to the health personnel.

References

Aisa-Alvarez A., Soto M.E., Guarner-Lans V., Camarena-Alejo G., Franco-Granillo J., Martínez-Rodríguez E.A., Gamboa Á.R., Manzano-Pech L. and Pérez-Torres I. (2020). Usefulness of antioxidants as adjuvant therapy for septic shock: A randomized clinical trial. Medicina (Kaunas) 56, 619.

Anand S.K. and Tikoo S.K. (2013). Viruses as modulators of mitochondrial functions. Adv. Virol. 2013, 738794.

Archer S.L., Sharp W.W. and Weir E.K. (2020). Differentiating COVID-19 pneumonia from acute respiratory distress syndrome and high altitude pulmonary edema: Therapeutic implications circulation. Circulation 142, 101-104.

Arosio P. and Levi S. (2002). Ferritin, iron homeostasis, and oxidative damage. Free. Radic. Biol. Med. 33, 457-463.

Aubert M., Pomeranz L.E. and Blaho J.A. (2007). Herpes simplex virus blocks apoptosis by precluding mitochondrial cytochrome c release independent of caspase activation in infected human epithelial cells. Apoptosis 12, 19-35.

Battaglia A.M., Chirillo R., Aversa I., Sacco A., Costanzo F. and Biamonte F. (2020). Ferroptosis and cancer: Mitochondria meet the "iron maiden" Cell Death Cells. 9,1505.

Brealey D., Brand M., Hargreaves I., Heales S., Land J., Smolenski R., Nathan A.D., Chris E.C. and Mervyn S. (2002). Association between mitochondrial dysfunction and severity and outcome of septic shock. Lancet 360, 219-223.

Chan C.P., Siu K.L., Chin K.T., Yuen K.Y., Zheng B. and Jin D.Y. (2006). Modulation of the unfolded protein response by the severe acute respiratory syndrome coronavirus spike protein. J. Virol. 80, 9279-9287.

Chavarría A.P., Vázquez R.R.V., Cherit J.G.D., Bello H.H., Suastegui H.C., Moreno-Castañeda L., Alanís E.G., Hernández F., González-Marcos O., Saucedo-Orozco H., Manzano-Pech L., Márquez-Velasco R., Guarner-Lans V., Pérez-Torres I. and Soto M.E. (2021). Antioxidants and pentoxifylline as coadjuvant measures to standard therapy to improve prognosis of patients with pneumonia by COVID-

19. Comput. Struct. Biotechnol. J. 19, 1379-1390.

Codo A.C., Davanzo G.D., Monteiro L., Nakaya H.I., Farias A.S. and Moraes-Vieira P.M. (2020). Elevated glucose levels Elevated Glucose Levels Favor SARS-CoV-2 Infection and Monocyte Response through a HIF-1a/ Glycolysis-Dependent. Cell. Metabolism. 32, 437-446.

Davies J.P., Almasy K.M., McDonald E.F. and Plate L. (2020). Comparative multiplexed interactomics of SARS-CoV-2 and homologous coronavirus non-structural proteins identifies unique and shared host-cell dependencies. ACS Infect. Dis. 6, 3174-3189.

Delgado-Roche L. and Mesta F. (2020). Oxidative stress as key player in severe acute respiratory syndrome Coronavirus (SARS-CoV) Infection. Arch. Med. Res. 51, 384-387.

Edeas M., Jumana S. and Peyssonnaux C. (2020). Iron: innocent bystander or vicious culprit in COVID-19 pathogenesis? Int. J. Infect. Dis. 97, 303-305.

García-Yébenes I., García-Culebras A., Peña-Martínez C., Fernández-López D., Díaz G.J., Negredo P., Avendaño C., Castellanos M., Gasull T., Dávalos A., Moro M.A. and Lizasoain I. (2018). Iron overload exacerbates the risk of hemorrhagic transformation after TPA (tissue-type plasminogen activator) administration in thromboembolic stroke mice. Stroke 49, 2163-2172.

Glingston S.R., Deb R., Kumar S. and Nagotu S. (2019). Organelle dynamics and viral infections: at cross roads. Microbes. Infect. 21, 20-32.

Guler N., Siddiqui F. and Fareed J. (2020). Is the reason of increased D-Dimer levels in COVID-19 because of ACE-2-induced apoptosis in endothelium? Clin. Appl. Thromb. Hemost. 26, 1076029620935526.

Hartmann A., Michel P.P., Troadec J.D., Mouatt-Prigent A., Faucheux B.A., Ruberg M., Agid Y. and Hirsch E.C. (2001). Is Bax a mitochondrial mediator in apoptotic death of dopaminergic neurons in Parkinson's disease? J. Neurochem. 76, 1785-1793.

Hee J.S. and Cresswell P. (2017). Viperin interaction with mitochondrial antiviral signaling protein (MAVS) limits viperin-mediated inhibition of the interferon response in macrophages. PLoS One 12, e0172236.

Herst P.M., Rowe M.R., Carson, G.M. and Berridge M.V. (2017). Functional mitochondria in health and disease Front. Endocrinol. (Lausanne) 8, 296.

Huang F., Huang M., Zhang H., Zhang C., Zhang D. and Zhou G. (2016). Changes in apoptotic factors and caspase activation pathways during the postmortem aging of beef muscle. Food. Chem. 190, 110-114.

Ibrahim I.M., Abdelmalek D.H., Elshahat M.E. and Elfiky A.A. (2020). COVID-19 Spike-host cell receptor GRP78 binding site prediction. J. Infect. 80, 554-562.

Ince C. (2005). The microcirculation is the motor of sepsis. Crit. Care 9, S13-S19.

Jacobs W., Lammens M., Kerckhofs A., Voets E., Van San E., Van Coillie S., Peleman C., Mergeay M., Sirimsi S., Matheeussen V., Jansens H., Baar I., Berghe T.V. and Jorens P.G. (2020). Fatal lymphocytic cardiac damage in coronavirus disease 2019 (COVID-19): autopsy reveals a ferroptosis signature ESC. Heart Fail. 7, 3772-3781.

Jean-Beltran P.M., Cook K.C. and Cristea I.M. (2017). Exploring and exploiting proteome organization during viral infection. J. Virol. 91, e00268-e00217.

Jouihan H.A., Cobine P.A., Cooksey R.C., Hoagland E.A., Boudina S., Abel E.D., Winge D.R. and McClain D.A. (2008). Iron-mediated inhibition of mitochondrial manganese uptake mediates

mitochondrial dysfunction in a mouse model of hemochromatosis. Mol. Med. 14, 98-108.

Kapadia S.B. and Chisari F.V. (2005). Hepatitis C virus RNA replication is regulated by host geranylgeranylation and fatty acids. Proc. Natl. Acad. Sci. USA 102, 2561-2566.

Khan M., Syed G.H., Kim S.J. and Siddiqui A. (2015). Mitochondrial dynamics and viral infections: a close nexus. Biochim. Biophys. Acta 1853, 2822-2833.

Koshiba T., Yasukawa K., Yanagi Y. and Kawabata S. (2011). Mitochondrial membrane potential is required for MAVS-mediated antiviral signaling. Sci. Signal. 158, ra7.

Kwong J.Q. and Molkentin J.D. (2015). Physiological and pathological roles of the mitochondrial permeability transition pore in the heart. Cell. Metab. 21, 206-214.

Lane D.J.R., Merlot A.M., Huang M.L.H., Bae D.H., Jansson, P.J., Sahni, S., Kalinowski D.S. and Richardson D.R. (2015). Cellular iron uptake, trafficking and metabolism: key molecules and mechanisms and their roles in disease. Biochim. Biophys. Acta 1853, 1130-1144.

Levi M., Thachil J., Iba T. and Levy J.H. (2020). Coagulation abnormalities and thrombosis in patients with COVID-19. Lancet Haematol. 6, e438-e440.

Levy R.J. and Deutschman C.S. (2007). Cytochrome c oxidase dysfunction in sepsis. Crit. Care Med. 35, S468-S475.

Li X., Fang P., Mai J., Choin E.T., Wang H. and Yang X.F. (2013). Targeting mitochondrial reactive oxygen species as novel therapy for inflammatory diseases and cancers. J. Hematol. Oncol. 6, 19.

Lu L.F., Li S., Lu X.B., LaPatra S.E., Zhang N., Zhang X.J., Chen D.D., Nie P. and Zhang Y.A. (2016). Spring viremia of carp virus N protein suppresses fish IFNφ1 production by targeting the mitochondrial antiviral signaling protein. J. Immunol. 196, 3744-3753.

Luna-López A., López-Diazguerrero N.E., González-Puertos V.Y., Triana-Martínez F. and Königsberg-Fainstein M. (2008). El fantástico mundo de la proteína Bcl-2. REB. Revista de Educación Bioquímica 27, 93-102.

Luo P., Qiu L., Liu Y., Liu X.-L., Zheng J.-L., Xue H.-Y., Liu W.-H., Liu D. and Li J. (2020). Metformin treatment was associated with decreased mortality in COVID-19 patients with diabetes in a retrospective analysis. Am. J. Trop. Med. Hyg.103, 69-72.

Mailloux R.J. (2018). Mitochondrial antioxidants and maintenance of cellular hydrogen peroxide levels. Oxid. Med. Cell. Longev. 2018, 1-10.

Malgorzata K., Ghobrial R.M. and Kubiak J.Z. (2020). The Role of genetic sex and mitochondria in response to COVID-19 infection. Int. Arch. Allergy Immunol. 181, 629-634.

Melser S., Lavie J. and Bénard G. (2015). Mitochondrial degradation and energy metabolism. Biochim. Biophys. Acta 1853, 2812-2821.

Mills E.L., Kelly B. and O'Neill L.A.J. (2017). Mitochondria are the powerhouses of immunity. Nat. Immunol. 18, 488-498.

Mittal M., Siddiqui M.R., Tran K., Reddy S.P. and Malik A.B. (2014). Reactive oxygen species in inflammation and tissue injury. Antioxid. Redox Signal. 20, 1126-1167.

Onoue S., Kumon Y., Igase K., Ohnishi T. and Sakanaka M. (2005). Growth arrest and DNA damage-inducible gene 153 increases transiently in the thalamus following focal cerebral infarction. Brain. Res. Mol. Brain. Res. 134, 189-197.

Pal R. (2020). COVID-19, hypothalamo-pituitary-adrenal axis and clinical implications. Endocrine 68, 251-252.

Pal R. and Banerjee M. (2020). COVID-19 and the endocrine system: exploring the unexplored. J. Endocrinol. Invest. 43, 1027-1031.

Paul B.T., Manz D.H., Torti F.M. and Torti S.V. (2017). Mitochondria and Iron: current questions. Expert. Rev. Hematol. 10, 65-79.

Paumard P.J., Vaillier J., Coulary B., Schaeffer J., Soubannier V., Mueller D.M., Brèthes D., di Rago J.P. and Velours J. (2002). The ATP synthase is involved in generating mitochondrial cristae morphology. EMBO J. 21, 221-230.

Pérez-Torres I., Manzano-Pech L., Rubio-Ruíz M.E., Soto M.E. and Guarner-Lans V. (2020). Nitrosative stress and its association with cardiometabolic disorders. Molecules 25, 2555.

Petersen J.M., Her L.S. and Dahlberg J.E. (2001). Multiple vesiculoviral matrix proteins inhibit both nuclear export and import. Proc. Natl. Acad. Sci. USA 98, 8590-8595.

Qu C., Zhang S., Li Y., Wang Y., Peppelenbosch M.P. and Pan Q. (2019). Mitochondria in the biology, pathogenesis, and treatment of hepatitis virus infections. Rev. Med. Virol. 29, e2075.

Ramiere C., Rodriguez J., Enache L.S., Lotteau V., Andre P. and Diaz O. (2014). Activity of hexokinase is increased by its interaction with hepatitis C virus protein NS5A. J. Virol. 88, 3246-3254.

Rongvaux A., Jackson R., Harman C.C., Li T., West A.P., R de Zoete M., Wu Y., Yordy B., Lakhani S.A. and Kuan C.Y. (2014). Apoptotic caspases prevent the induction of type I interferons by mitochondrial DNA Cell. 159, 1563-1577.

Rumora A.E., Lentz S.I., Hinder L.M., Jackson S.W., Valesano A., Levinson G.E. and Feldman E.L. (2018). Dyslipidemia impairs mitochondrial trafficking and function in sensory neurons. FASEB J. 32, 195-207.

Sakaida I., Kimura T., Yamasaki T., Fukumoto Y., Watanabe K., Aoyama M. and Okita K. (2005). Cytochrome c is a possible new marker for fulminant hepatitis in humans. J. Gastroenterol. 40, 179-185.

Segal M.S. and Beem E. (2001). Effect of pH, ionic charge, and osmolality on cytochrome c-mediated caspase-3 activity. Am. J. Physiol. Cell. Physiol. 281, C1196-C1204.

Simmons J.D., Lee Y.L., Pastukh V.M., Capley G., Muscat C.A., Muscat D.C., Marshall M.L., Brevard S.B. and Gillespie M.N. (2017). Potential contribution of mitochondrial DNA damage associated molecular patterns in transfusion products to the development of acute respiratory distress syndrome after multiple transfusions J. Trauma. Acute Care Surg. 82, 1023-1029.

Singh K.K., Chaubey G., Chen J.Y. and Suravajhala P. (2020). Decoding SARS-CoV-2 hijacking of host mitochondria in COVID-19 pathogenesis. Am. J. Physiol. Cell. Physiol. 319, C258-C267.

Singhal A.T. (2020). Review of coronavirus disease-2019 (COVID-19). Indian. J. Pediatr. 87, 281-286.

Simonart T., Boelaert J.R., Mosselmans R, Andrei G., Noel J.C, De Clercq E. and Snoeck R. (2002). Antiproliferative and apoptotic effects of iron chelators on human cervical carcinoma cells. Gynecol. Oncol. 85, 95-102.

Soto M.E., Guarner-Lans V., Soria-Castro E., Manzano-Pech L. and Pérez-Torres I. (2020). Is antioxidant therapy a useful complementary measure for Covid-19 treatment? An algorithm for its application. Medicina (Kaunas) 56, E386.

Thachil J. (2020). The protective rather than prothrombotic fibrinogen in COVID-19 and other inflammatory states. J. Thromb. Haemost. 18, 1849-1852.

Williamson C.D., DeBiasi R.L. and Colberg-Poley A.M. (2012). Viral product trafficking to mitochondria, mechanisms and roles in pathogenesis. Infect. Disord. Drug. Targets 12, 18-37.

Wu K.E., Fazal F.M., Parker K.R., Zou J. and Chang H.Y. (2020). RNA-

GPS predicts SARS-CoV-2 RNA residency to host mitochondria and nucleolus. Cell. Syst. 11, 102-108.

Yang M. and Lai C.L. (2020). SARS-CoV-2 infection: can ferroptosis be a potential treatment target for multiple organ involvement? Cell Death. Discov. 6, 130.

Yin X., Li X., Ambardekar C., Hu Z., Lhomme S. and Feng Z. (2017). Hepatitis E virus persists in the presence of a type III interferon response. PLoS Pathog.13, e1006417.

Young A., Oldford C. and Mailloux R.J. (2020). Lactate dehydrogenase supports lactate oxidation in mitochondria isolated from different mouse tissues. Redox Biol. 28, 1-7.

Zhang W., Han P., Zhang J., Zhu Y., Meng X., Zhang J., Hu Y., Yi Z. and Wang R. (2019). Influenza A virus (H1N1) triggers a hypoxic response by stabilizing hypoxia-inducible factor-1α via Inhibition of proteasome. Virology 530, 51-58.

Zhang Y., Xiao M., Zhang S., Xia P., Cao W., Jiang W., Chen H., Ding X., Zhao H., Zhang H., Wang C., Zhao J., Sun X., Tian R., Wu W., Wu D., Ma J., Chen Y., Zhang D., Xie J., Yan X., Zhou X., Liu Z., Wang J., Du B., Qin Y., Gao P., Qin X., Xu Y., Zhang W., Li T., Zhang F., Zhao Y., Li Y. and Zhang S. (2020). Coagulopathy and antiphospholipid antibodies in patients with Covid-19. N. Engl. J. Med. 382, e38.

Zhou Y., Frey T.K. and Yang J.J. (2009). Viral calciomics: Interplays between Ca^{2+} and virus. Cell Calcium 46, 1-17.